Flexible Silk–Inorganic Nanocomposites: From Transparent to Highly Reflective

By *Eugenia Kharlampieva, Veronika Kozlovskaya, Ray Gunawidjaja, Valeriy V. Shevchenko, Richard Vaia, Rajesh R. Naik, David L. Kaplan,* and *Vladimir V. Tsukruk**

A novel type of all-natural, biocompatible, and very robust nanoscale free-standing biohybrids are reported. They are obtained by integrating a silk fibroin matrix with functional inorganic nanoplatelets using a spin-assisted layer-by-layer assembly. The organized assembly of the silk fibroin with clay (montmorillonite) nanosheets results in highly transparent nanoscale films with significantly enhanced mechanical properties, including strength, toughness, and elastic modulus, as compared to those for the pristine silk nanomaterials. Moreover, replacing clay nanoplatelets with a highly reflective Langmuir monolayer of densely packed silver nanoplates causes a similar enhancement of the mechanical properties, but in contrast to the materials above, highly reflective, mirror-like, nanoscale flexible films are created. This strategy offers a new perspective for the fabrication of robust all-natural flexible nanocomposites with exceptional mechanical properties important for biomedical applications, such as reinforced tissue engineering. On the other hand, the ability to convert silk-based nanoscale films into mirror-like biocompatible flexible films can be intriguing for prospective photonics and optical exploitation of these nanobiohybrids.

1. Introduction

The demand for biocompatible composite materials that are mechanically strong and possess unique electronic and photonic properties inspires researchers towards bio-inorganic nanohybrids where biomolecules are utilized as soft and flexible organic matrices for the incorporation of functional inorganic moieties.[1–3] Among the variety of modern biomaterials, silk fibroin has attracted great attention because of its biocompatibility, biodegradability, and extraordinary physical properties. This combination makes silk materials attractive for applications in different fields including tissue engineering and biomechanical applications.[4–6] For example, silk possesses excellent mechanical properties (high elastic modulus and high elongation-to-break)[7–11] combined with near-perfect transparency in the visible range. Another remarkable feature of silk materials is their surface smoothness, which is a result of all-aqueous silk processing.[4] Several approaches have been developed to enhance the optical, biocompatible, antimicrobial, and thermal properties of silk.[12–23] Despite silk being one of the strongest biomaterials, it still lacks sufficient mechanical robustness for demanding applications. Therefore, different inorganic fillers such as silica, titania, zirconia, apatite, carbon nanotubes, or metal nanoparticles have been utilized as reinforcing agents.[24–27]

Previous studies on silk reinforcement have mostly focused on silk composites, such as cast films, blends, or fibers, all with microscopic dimensions. However, nanoscale free-standing films ($\leq$100 nm), which would be beneficial for a wide range of sensing applications because of their light weight, flexibility, and scalability, have thus far not been considered.[28–30] These robust ultrathin flexible films when freely suspended have shown a high sensitivity and dynamic range with potential applications as pressure and temperature sensor arrays.[31,32] The most promising fabrication approach for such nanofilms is a layer-by-layer (LbL) assembly.[33,34] Silk fibroin has also been exploited for the assembly of nanoscale films,[35] whereby these nanoscale films exhibited excellent mechanical properties with a Young's modulus and toughness of up to 8 GPa and 300 kJ m^{-3}, respectively.[36]

[*] Prof. V. V. Tsukruk, Dr. E. Kharlampieva, Dr. V. Kozlovskaya, Dr. R. Gunawidjaja
School of Materials Science and Engineering
Georgia Institute of Technology
Atlanta, GA 30332 (USA)
E-mail: vladimir@mse.gatech.edu
Prof. V. V. Shevchenko
Institute of Macromolecular Chemistry
National Academy of Science of Ukraine
Kiev 02160 (Ukraine)
Dr. R. R. Naik, Dr. R. Vaia
Air Force Research Laboratory
Materials and Manufacturing Directorate
Wright-Patterson AFB
Dayton, OH 45433-7750 (USA)
Prof. D. L. Kaplan
Department of Biomedical Engineering
Tufts University
Medford, MA 02155 (USA)

DOI: 10.1002/adfm.200901774

WILEY InterScience® DISCOVER SOMETHING GREAT
© 2010 WILEY-VCH Verlag GmbH & Co. KGaA, Weinheim

To date LbL has been utilized for a variety of synthetic and biological materials and inorganic moieties such as nanoparticles, nanosheets, and nanowires.[31,37–42] One of the intriguing examples, published by Kotov and co-workers, involved the fabrication of ultrastrong macroscopic films via the LbL incorporation of clay—a layered silicate material with a high inherent in-plane tensile stiffness reaching 270 GPa.[43,44] Introducing additional cross-linking into 1–1.5-μm-thick clay–polyelectrolyte composites effected an increase in the Young's modulus of up to 106 ± 11 GPa.[45–47] Apart from outstanding mechanical properties, LbL clay–polyelectrolyte films have also shown good antimicrobial[48] and cell-adhesive properties,[49] as well as a significant increase in their ion conductivity.[50]

In the present study, we attempt to integrate an ultrathin and highly transparent LbL silk matrix with functional inorganic moieties to tune the mechanical and optical properties of the nanocomposites. For that purpose we utilized individually dispersed, aluminosilicate layers of montmorillonite (MMT) and silver nanoplatelets as reinforcing agents. The materials are biocompatible and provide excellent mechanical strength and toughness, large surface-area-to-mass ratios, and a high degree of flexibility; they can be processed from environmentally friendly aqueous solutions. To fabricate the free-standing nanocomposites, we performed a bottom-up assembly of the silk fibroin and nanoplates using two approaches: a spin-assisted LbL (SA LbL)[36] and a Langmuir–Blodgett (LB) method. The SA LbL approach comprised a combination of conventional LbL and spin-coating as a way to construct free-standing, well-organized, ultrathin films of high mechanical strength.[51–54] The LB technique has been proven to be a powerful tool for the nanoscale assembly of highly ordered monolayers at air/water interfaces.[55] Thus, silk$_n$ or (silk–MMT)$_n$ films were fabricated by alternating LbL deposition from silk and clay solutions; whereas the nanohybrids of silk and the silver nanoplates (AgNPL) were constructed by incorporating a Langmuir monolayer of silver nanoplates in between the silk LbL matrices (Fig. 1).

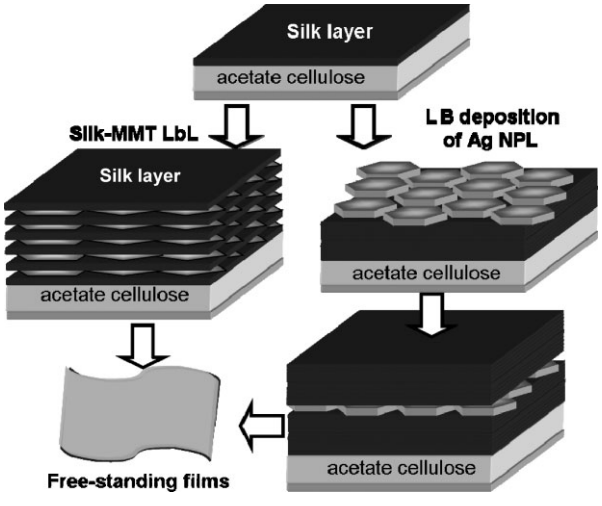

Figure 1. Reinforced silk nanocomposites of LbL (silk–MMT)$_n$ films are obtained by alternating deposition of silk and MMT layers, while silk$_m$–AgNPL–silk$_m$ films are constructed by incorporating a Langmuir monolayer of silver nanoplates in between the silk LbL matrices.

The reported results include: a) the fabrication and characterization of the silk–clay and silk–silver nanoplate nanomembranes; b) the testing performance of the nanocomposites as mechanically robust ultrathin membranes; and c) the evaluation of the optical properties of the films. We found that the ultrathin silk–inorganic nanocomposites demonstrated unique mechanical properties, such as a three-times higher toughness and Young's modulus compared to those of pristine LbL silk nanofilms. In addition, depending on the inorganic reinforcement, the ultrathin silk composites can be highly transparent or highly reflective and mirror-like. To the best of our knowledge, this is the first example of ultrathin, biocompatible, free-standing, and mechanically robust nanofilms with tailored optical properties.

2. Results and Discussion

We found that the SA LbL assembly of silk fibroin with clay nanoplatelets was successful and a linear growth starting from the fifth bilayer was found with an individual thickness of 5 ± 0.5 nm and 1.3 ± 0.2 nm for the silk and clay layers, respectively (Fig. 2a). The thickness of the clay component corresponds to the thickness of an individual aluminosilicate layer of montmorillonite,[43] and indicates that monolayer formation occurs upon adsorption (Fig. 2a). Indeed, transmission electron microscopy (TEM) analysis showed clay platelets of a few hundred nanometers across, and atomic force microscopy (AFM) images indicated a full integration of the clay nanoplatelets into the silk matrix with a resulting smooth surface (microroughness of about 2.7 nm, which is comparable to that for the pure silk film; Fig. 2b–d).[36]

To confirm the presence of the clay nanoparticles, the organic matrix was exposed to 500 °C. This treatment uncovered MMT nanoparticles with average lateral dimensions of 200 nm

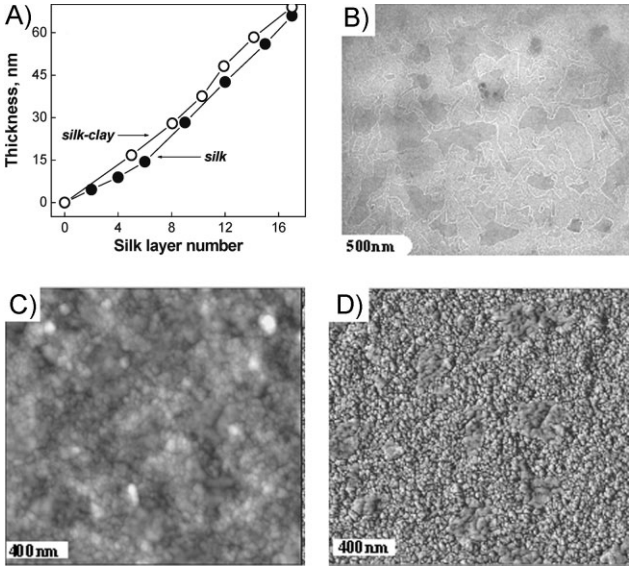

Figure 2. A) The thickness increase for (silk)$_n$ and (silk–MMT)$_n$ films with increasing number (n) of deposited layers. The experimental error in the top panel is within the symbol size. B) TEM of a (silk–MMT)$_{12}$ film. C,D) AFM topographical (C) and phase images (D) of a (silk–MMT)$_{12}$ film. The height in (C) is 40 nm, and the z-scale in (D) is 10°.

© 2010 WILEY-VCH Verlag GmbH & Co. KGaA, Weinheim

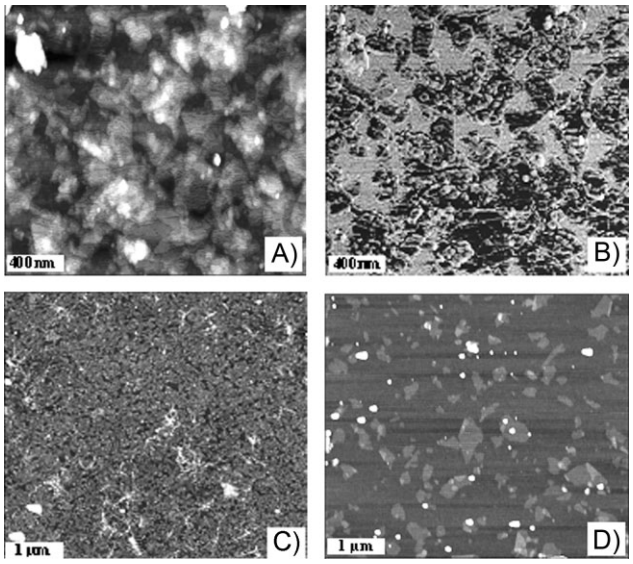

Figure 3. A,B) AFM topographical (A) and phase images (B) of a (silk–MMT)$_{12}$ film after treatment at 500 °C. The height in (A) is 10 nm and the *z*-scale in (B) is 50°. C,D) AFM topographical images of a (silk–MMT)$_1$ film before (C) and after treatment at 500 °C (D). The height is 20 nm in (C) and the *z*-scale in (D) is 10°.

distributed over the substrate (Fig. 3a,b). Independently, the clay particles were deposited on a poly(allylamine hydrochloride) (PAH)-topped surface to confirm whether the nanoplatelets were well-dispersed in solution and did not form large microscopic aggregates. The deposited clay particles existed as irregular sheetlike structures that were around 1 nm thick and up to 200 nm wide in the other dimensions, which correlates well with previously found values for clay[43] (data not shown). To determine the surface coverage within a single layer (silk–MMT)$_1$ was exposed to a temperature of 500 °C. The result revealed that MMT adsorbed from a 0.05% solution covers only around 8% of the surface area (Fig. 3c,d). The low coverage of MMT on the silk surface as compared to that of around 80% on a PAH layer reflects the lower charge density of the silk surface and its much higher hydrophobicity at neutral pH as compared to PAH (p*I* of around 4).[56]

The buckling instability under compression and the stress–strain data from bulging experiments enabled the determination of the compressive and tensile mechanical properties of the pristine silk and silk–MMT nanocomposite films (Table 1 and

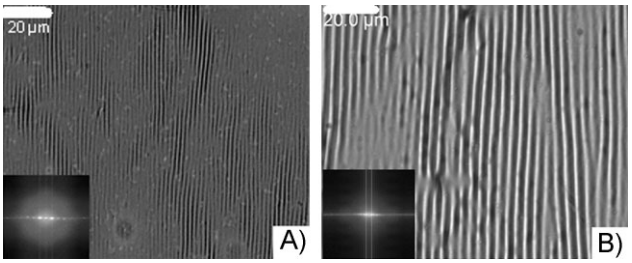

Figure 4. Optical images of the compressed films: A) (silk)$_{17}$ and B) (silk–MMT)$_{17}$ on PDMS substrates. The insets show the corresponding 2D Fourier Transform (FT) images utilized for the spacing evaluation.

Fig. 4 and 5).[36,57,58] We found that despite of the low content of the clay nanoplatelets within the silk matrix (0.6% of the volume fraction), the incorporation of clay had a dramatic effect on the mechanical properties. The 70-nm-thick (silk–MMT)$_{17}$ films showed outstanding mechanical properties represented by a threefold increase in the elastic modulus to 12 ± 2 GPa, a twofold increase in the mechanical strength to 120 MPa, and a fourfold increase in the overall toughness to 950 ± 100 kJ m^{-3} as compared to the unreinforced silk membranes (Table 1). The values for the 50-nm pristine silk membranes correlated well with those published earlier for the 85-nm films.[36] However, a further increase in the clay concentration (1%) resulted in brittle, filled silk films. On the other hand, even a 0.3% volume fraction of clay increased the elastic modulus and toughness already by a factor of two as compared to initial values for silk films of comparable thickness (Table 1). These results indicate that the mechanical strength of the nanocomposites reaches an optimum value at 0.6% volume fraction. In contrast, to achieve similar mechanical properties in the conventional bulk clay–polymer composite (non-crosslinked) films, a much higher clay content (close to around 10 wt%) and films of an order of magnitude of two thicker must be incorporated.[44,59] Moreover, the enhancement of the mechanical properties indicates a good compatibility of the silk and clay materials. The results are in contrast to earlier reports of microscopic composites of clay with chitosan, another naturally strong polymer, which showed a threefold higher elastic modulus but a significantly reduced toughness (by about 30%).[60]

A further increase in the elastic modulus up to 18 ± 2 GPa was achieved by post-treatment of the silk–clay films with methanol. This even more significant fivefold increase can be attributed to the formation of ß-sheets and a partial silk crystallization induced by

Table 1. Mechanical properties of silk-based nanocomposite films as measured by buckling and bulging techniques.

	Filler volume fraction [%]	Film thickness [nm]	Bulging Young's modulus [GPa]	Buckling Young's modulus [GPa]	Ultimate stress [MPa]	Ultimate strain [%]	Toughness [kJ m^{-3}]
Silk$_{12}$	0	49 ± 2	4.2 ± 1.3	3.6 ± 1.2	60–100	0.5–1.0	200 ± 100
(Silk–MMT)$_{12}$	0.3	50 ± 2	8 ± 2	5.7 ± 1.2	90–100	0.7–1.0	400 ± 70
(Silk–MMT)$_{12}$	0.6	50 ± 2	10 ± 2	8 ± 2	80 ± 20	0.7–1.0	400 ± 50
(Silk–MMT)$_{17}$	0.6	70 ± 2	12 ± 2	10.7 ± 1.3	100 ± 20	1.1	950 ± 100
(Silk–MMT)$_{17,}$ (MeOH),	0.6	70 ± 2	18 ± 2	16.2 ± 1.8	100 ± 10	0.9	720 ± 50
Silk$_{10}$- AgNPL-Silk$_{10}$	20	110 ± 5	14 ± 2	12 ± 3	70 ± 5	1.0 ± 0.1	500 ± 50
Silk$_{10}$- AgNPL-Silk$_{10,}$ (MeOH)	20	110 ± 5	16 ± 2	n/a	98 ± 6	0.9 ± 0.1	330 ± 70

WILEY InterScience® DISCOVER SOMETHING GREAT
© 2010 WILEY-VCH Verlag GmbH & Co. KGaA, Weinheim

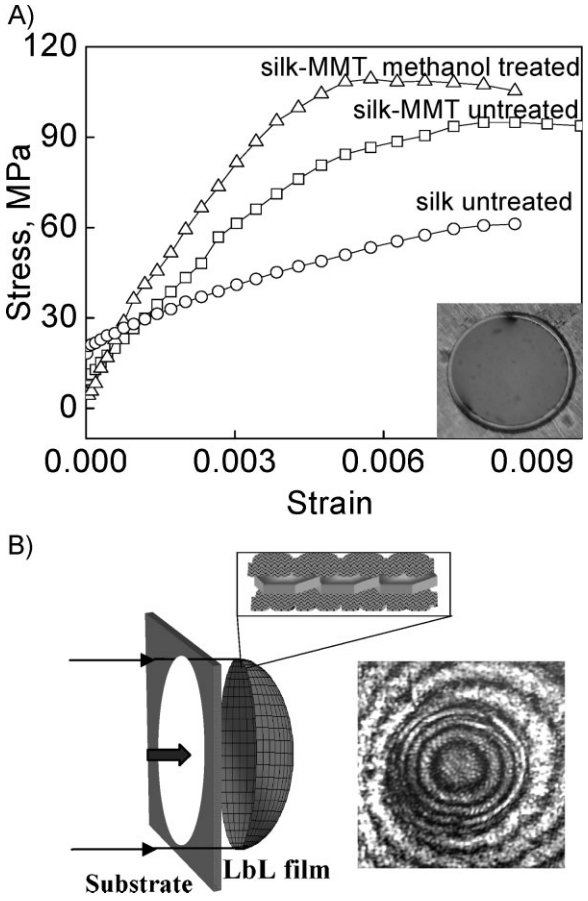

Figure 5. A) Stress–strain data for the $(silk)_{17}$ (circles) and $(silk–MMT)_{17}$ films (triangles and squares) under different conditions. The inset shows a representative optical microscopy image of the $(silk–MMT)_{17}$ LbL films suspended over a 150 μm diameter opening. B) A schematic representation of the bulging test (left) and the interference pattern of a $(silk–MMT)_{17}$ film suspended over a 150 μm opening under 4000 Pa (right).

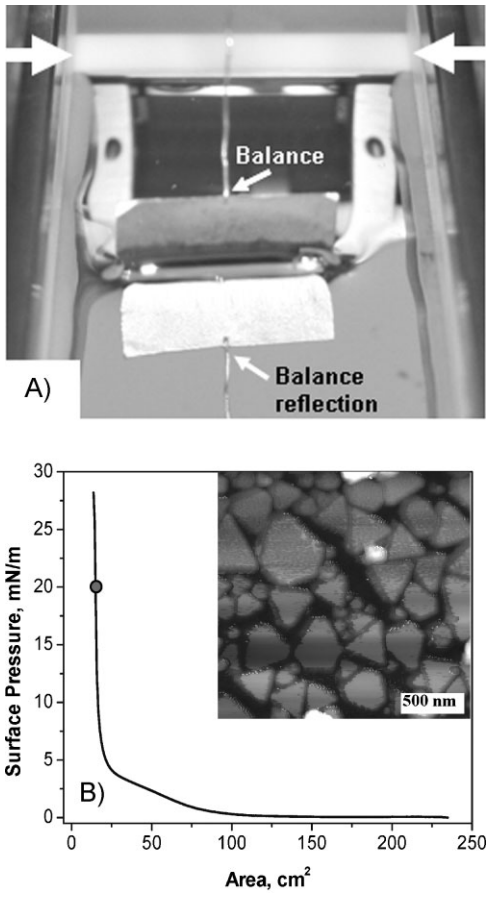

Figure 6. A) An LB trough with a AgNPL monolayer at the water–air interface after compression (indicated by the large arrows). The clear reflection of the balance illustrates the highly reflective surface of the monolayer. B) A Langmuir isotherm of the AgNPL monolayer. The dot represents the surface pressure (20 mN m^{-1}) at which the AgNPL monolayer was transferred onto the solid substrate. The inset shows an AFM image of the monolayer transferred on a $(silk)_{10}$ film.

the methanol.[36] At the same time, the toughness was slightly lower (720 ± 50 kJ m^{-3}) than that for the films before methanol treatment (950 ± 100 kJ m^{-3}). Such behavior has previously been seen in polymer–clay composites where the toughness gradually decreases with increasing elastic modulus.[45] It is worth noting that values obtained from the buckling experiments are consistently lower than those obtained from the bulging tests (Table 1). The results correlate well with the previous findings and can be explained by a different mechanism of the deformation of platelets under the compression and tensile deformations.[36]

As an alternative approach to reinforce the nanoscale silk films, we explored the incorporation of silver nanoplates into a silk matrix. This approach also introduced opportunities to dramatically change the optical properties of these nanocomposite films because of the strong reflective properties of the silver nanoplates. The incorporation was achieved by "sandwiching" a Langmuir monolayer of silver nanoplates into an LbL matrix as described above (Fig. 1). The $silk_{10}$–AgNPL–$silk_{10}$ nanoscale films with a total thickness of around 110 nm were constructed by including silver nanoplates (30 nm thickness) between two multilayers of the LbL-assembled silk (40 nm each; Fig. 1). The Langmuir isotherm indicates the formation of a dense monolayer of silver nanoplates (Fig. 6). An optical image of the Langmuir monolayer shows highly reflective properties with a clear mirror image of the balance (Fig. 6). An AFM image of the complete silk–AgNPL films shows a modest surface microroughness of 6 nm and the densely packed triangular silver nanoplates (Fig. 6).

The silk–AgNPL films preserve their mirror-like reflective properties after being released as free-standing films (Fig. 7a). The free-standing films were very robust and were easily transferred to TEM grids. TEM analysis of the films revealed the dense packing of the silver nanoplates with a surface coverage of around 85% (Fig. 7b). The somewhat irregular sizes and shapes of the nanoplates (50–400) nm seem to be very beneficial for their tight packing, where the smaller nanoparticles are filling the gaps between the larger ones.

Remarkably, the silk–AgNPL films showed an elastic modulus of 14 ± 2 GPa which is an approximately fourfold increase of that of the pristine silk films and slightly higher than that observed for the silk–clay nanocomposites of comparable thickness (12 ± 2 GPa).

© 2010 WILEY-VCH Verlag GmbH & Co. KGaA, Weinheim

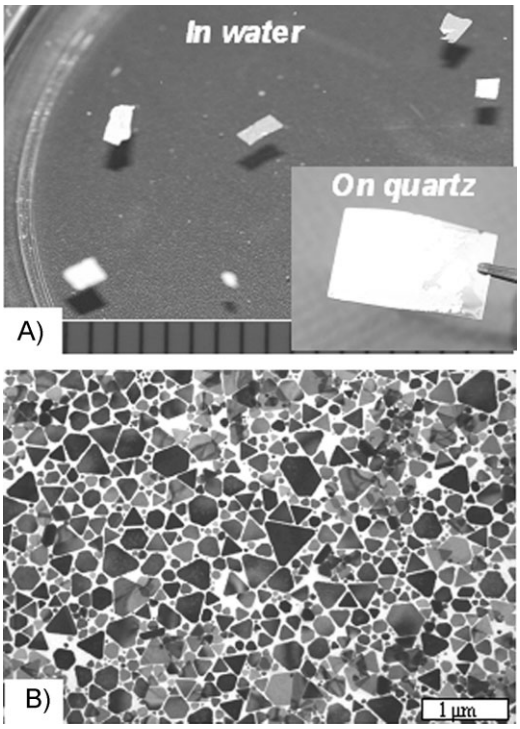

Figure 7. Optical (A) and TEM (B) images of free-standing $silk_{10}$–AgNPL–$silk_{10}$ films. The inset in (A) shows the $silk_{10}$–AgNPL–$silk_{10}$ film on a quartz slide.

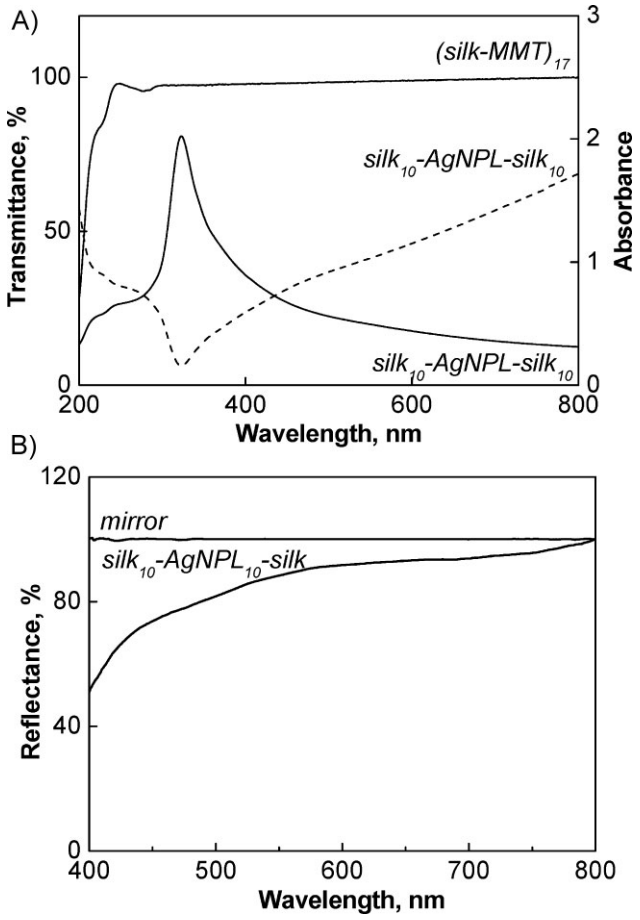

Figure 8. A) Transmission of $(silk–MMT)_{17}$ and $silk_{10}$-AgNPL-$silk_{10}$ films (solid lines). The absorbance of the $silk_{10}$-AgNPL-$silk_{10}$ film is shown as a dashed line. The films were deposited on quartz slides. B) Reflectance of a $silk_{10}$-AgNPL-$silk_{10}$ film. A common mirror was taken as the reference.

The toughness also increased twofold to 500 ± 50 kJ m^{-3} (Table 1). As expected, the methanol-treated silk–AgNPL films exhibited a higher modulus (16 ± 2 GPa) but lower toughness (330 ± 70 kJ m^{-3}). Therefore, it can be concluded that silk–AgNPL composites demonstrate significantly improved mechanical properties of the silk matrix combined with highly reflective, mirror-like optical properties.

It is worth noting that both silk–MMT and silk–AgNPL membranes showed a high stability in both organic and aqueous solutions for months. The stability of these membranes originates from the very strong interactions between the adjacent silk layers. The capability of silk materials to undergo an intermolecular self-assembly at their surfaces[35] resulting in robust one-component LbL silk membranes has been reported previously.[36] The driving force for this interaction was suggested to be a partial silk crystallization as a result of film drying in between the layers at the deposition step.[35] Indeed, silk deposited from aqueous solutions as silk I (random coil) is partially transferred into silk II (random coils + ß sheets) followed by the strengthening of interlayer interactions.[61] In the case of composite membranes, the additional interactions between silk and its counterparts contribute to the interlayer binding leading to reinforced mechanical properties. Moreover, our results indicate that methanol, which enhances crystallization of silk and induces chain rearrangement,[36] does not effect the silk/nanofiller interfaces as the methanol-treated films remain stable in solution for the same amount of time as the films without methanol treatment.

Finally, we explored the extent to which the optical properties of silk-based nanocomposite films can be tuned from fully transparent to fully reflective. UV–vis spectroscopy confirmed the silk–clay films to be highly transparent (up to 95%) at all wavelengths with a slight decrease for wavelengths below 300 nm as a result of the absorbance of the silk material at 228[61] and 260 nm[62] (Fig. 8a). In contrast, the silk–Ag film has almost no transparency in the UV–vis range, except at 330 nm (Fig. 8a). The low transparency is explained by a significant absorbance of silver nanoplates in the visible range as seen from the absorbance spectrum of the silk–Ag film (dashed line in Fig. 8a). The spectrum of the AgNPL film resembles that of silver nanoplatelets in solution and shows a double-peak resonance spectrum with a broad peak at 890 nm. Because of the wide distribution in the diameters of the nanoplates, the in-plane and out-of-plane dipole, and in-plane quadrupole resonances give rise to a broad halo between 300 and 1000 nm.

We also evaluated the reflectance properties of the free-standing silk–AgNPL membranes. Since silk has a near-perfect transparency in the visible and near-IR ranges, the silk matrix does not affect the properties of the silver nanoplatelets. We found that the films showed around 98% reflectance in the near-IR range (750–850 nm), which gradually decreased to around 90% in the red visible range (650 nm) and to 85% in the green (532 nm) region

WILEY InterScience® DISCOVER SOMETHING GREAT
© 2010 WILEY-VCH Verlag GmbH & Co. KGaA, Weinheim

(Fig. 8b). The gradual decrease of the reflectance at lower wavelengths (<500 nm) is caused by an increased scattering of the silver nanoplates with lateral dimensions within 50–400 nm.

3. Conclusions

We demonstrated novel types of robust, ultrathin, silk–inorganic nanocomposite membranes with enhanced mechanical and tunable optical properties. The alternating assembly of a silk protein with clay nanoplatelets resulted in highly transparent nanoscale films with significantly enhanced mechanical properties, including strength, toughness, and elastic modulus, which were all several times higher than that for the pristine silk nanomaterials. The ultrathin (70–110 nm) reinforced silk films demonstrated outstanding elastic moduli of up to 20 GPa and a toughness of up to 1000 kJ m^{-3}.

On the other hand, the incorporation of highly reflective and densely packed silver nanoplates into LbL silk composites caused a similar enhancement of the mechanical properties, but it created highly reflective, mirror-like, nanoscale flexible films of silk materials with thicknesses around 100 nm. This strategy offers a new perspective for the fabrication of robust biocompatible flexible nanocomposites with exceptional mechanical properties that may be important for biomedical applications, such as reinforced tissue engineering. The ability to convert silk-based nanoscale films into mirror-like flexible films can be interesting for further photonics applications and optical exploitation of these biohybrids.

4. Experimental

Materials: Silk-fibroin solutions were prepared from *Bombyx mori* silkworm cocoons as described previously [61]. Silk cocoons were obtained from *B. mori* silkworms raised on a diet of Silkworm Chow (Mulberry Farms, Fallbrook, CA). To remove the sericin proteins from the fibers, the silk cocoons were soaked at 3.3% (w/v) in a solution of 8 M urea containing 40 mM of Tris-SO_4 and 0.5 M of β-mercaptoethanol, and heated to 90 °C for 1 h using a water bath. The silk fibers were then removed and dried by centrifugation at 4000 rpm in a 50 mL tube. The dried silk fibers were subsequently dissolved in a 50 mL tube containing 9.3 M lithium bromide solution. The solution was then dialyzed against distilled water using Slide-a-Lyzer dialysis cassettes (MWCO 3 500, Pierce) at room temperature for 2 days to remove the salt. Ultrapure distilled water was used to dilute the aqueous solution to the desired working condition of 0.2–0.5% for thin film fabrication.

Montmorillonite (MMT, Cloisite Na) was supplied in powder form by Southern MMT Products, Inc. Montmorillonite belongs to a class of 2:1 phyllosilicates, which are nominally 1D crystals comprising covalently bonded aluminosilicate layers, around 0.96 nm thick, separated by a van der Waals interlayer, a gallery-containing charge-compensating alkali metal, or by earth cations. The charge per unit cell (generally between 0.5 and 1.3 for swellable smectites) originates from isomorphous substitution within the aluminosilicate layer (e.g., tetrahedral Si^{4+} by Al^{3+} or octahedral Al^{3+} by Mg^{2+}). The number of exchangeable interlayer cations, the cation exchange capacity (CEC), generally ranges between 60 and 140 milliequivalents (meq) per 100 g. Cloisite Na has a nominal unit cell formula of $Na_{0.66}[Si_{7.8}Al_{0.2}O_{16}][Al_{2.96}Fe_{0.45}Mg_{0.44}Ca_{0.02}O_4(OH)_4]$ and a CEC of 95 meq/100 g.

Silver nanoplates (AgNPL) were reduced from a silver nitrate salt precursor at elevated temperature in the presence of polyvinylpyrrolidone (PVP) capping agent in dimethylformamide (DMF), according to a known procedure [63]. Briefly, a 30 mL DMF solution of $AgNO_3$ (0.025 M) was added dropwise into a 60 mL DMF solution of PVP (0.05 M, $M_n = 40\,000$ g mol^{-1}) at room temperature. During addition, the solution mixture gradually turned dark orange. The solution mixture was sealed in an autoclave and heated to a constant temperature, 165 °C for 24 h. The final product was tan-brown and tended to aggregate into a mirror-like film on the wall of the flask. The particles were purified by removing the excess PVP via multiple cycles of washing, centrifugation, and re-dispersion in methanol. For LB assembly, the purified AgNPL were dispersed in chloroform to give a concentration of approximately 8–10 mg mL^{-1}. Nanopure water with a resistivity of 18.2 MΩ cm was used in all experiments.

Silk–Inorganic LbL Films: Multilayered silk films were obtained by alternating SA-LbL depositions as described previously [36]. Specifically, 30 μL of a 2 mg mL^{-1} silk aqueous solution were sequentially dropped on the silicon substrates and rotated for 20 s at 3000 rpm, rinsing twice with Nanopure water between the deposition steps. Silk–MMT assembly was carried out in a similar way from a 2 mg mL^{-1} silk and MMT aqueous solution. Thus, *n*-bilayer silk or silk–MMT films denoted as $(silk)_n$ or $(silk–MMT)_n$, respectively, were constructed. Free-standing films were fabricated by the initial deposition of a sacrificial layer of acetate cellulose from a 2% solution in dioxane followed by $(silk–MMT)_n$ assembly. The films were released from the silicon substrates by exposure to acetone for TEM studies. To examine the effect of the MMT content on the mechanical properties, 50-nm films with MMT volume fractions of 0.3%, 0.6%, and 1% were obtained using 0.025%, 0.05%, and 0.1% MMT solutions, respectively.

To fabricate the silk–AgNPL nanocomposites, an LB technique was used in addition to the spin-assisted deposition. First, a silk matrix was obtained by a SA-LbL assembly on a CA sacrificial layer. A monolayer of AgNPL, synthesized as described above, was then deposited onto the silk matrix from an LB trough. Finally, the silk–AgNPL hybrid matrix was coated with an additional stack of LbL silk films via spin-assisted deposition to maintain the symmetry. This way hybrid $silk_{10}$–AgNPL–$silk_{10}$ films were obtained with a thickness of 110 nm including two layers of silk (40 nm each) and a monolayer of AgNPL (30 nm in thickness). The LB deposition was performed on a KSV 2000 minitrough. To obtain a dense monolayer of AgNPL, 80 μL of the 8–10 mg mL^{-1} AgNPL solution in chloroform was deposited dropwise and uniformly across the water subphase.

Characterization: The film morphology was studied by a Dimension 3000 AFM microscope (Digital Instruments). The AFM images were collected in the tapping mode with silicon tips with a spring constant of 50 N m^{-1} according to the procedure adapted in our group [64,65]. The thicknesses of the films were measured with a spectroscopic ellipsometer M2000U (Woolam). TEM was performed with a JEOL 100CX-2 electron microscope at 100 kV.

Buckling Tests: These tests were conducted to evaluate the elastic moduli of LbL membranes from the elastic buckling instability [36]. Buckling was achieved by the compression of the LbL films deposited on a polydimethylsiloxane (PDMS) substrate in accordance with a known approach [66]. This method uses the strain-induced elastic buckling instability and can be applied to LbL films, as was demonstrated by Nolte et al. [67]. For an isotropic thin membrane, a uniform buckling pattern with a characteristic wavelength, *k*, is observed when it is subjected to a critical compressive stress. The spacing of this pattern is directly related to the elastic modulus. To initiate the buckling pattern, a 2 mm × 2 mm membrane piece was placed over a 0.6 cm × 0.6 cm × 0.4 cm PDMS substrate, which was slowly compressed in micrometer-sized increments. The compression was monitored under an optical microscope in differential interference contrast (DIC) mode adjusted for maximum contrast. The optical images were captured with a Leica MZ16 microscope in reflection mode. The typical humidity at which the buckling measurements were performed was between 25 and 50%. Fourier transformation of the digital images was performed to determine the buckling wavelength using ImageJ software.

Bulging Tests: These tests were performed using a custom-made interferometer equipped with a charge-coupled device (CCD) camera (Logitech) and a He–Ne laser ($k = 632.8$ nm). Pressures of up to 5000 Pa were exerted using a 60 mL syringe regulated by an automatic pump (Kent Scientific Inc.) and monitored with an automatic pressure gauge, DPM 0.1

© 2010 WILEY-VCH Verlag GmbH & Co. KGaA, Weinheim

(SI Pressure Instruments). The bulging test data were analyzed using a model for the elastic deformation of circular membranes, according to the procedure described previously [40,41]. The LbL membranes freely suspended over a copper substrate with a 150-μm hole were first inspected under an optical microscope and a minimal pressure was exerted to check for symmetrical Newton's ring patterns that indicate membrane homogeneity [36].

Acknowledgements

This work was supported by the Air Force Office of Scientific Research, the Air Force Research Lab, the National Science Foundation, and the Office of Naval Research.

Received: September 19, 2009
Revised: October 25, 2009
Published online: February 16, 2010

[1] K. Ariga, A. Vinu, M. Miyahara, *Curr. Nanosci.* **2006**, *2*, 197.
[2] E. P. Giannelis, *Adv. Mater.* **1996**, *8*, 29.
[3] L. Chunmei, D. L. Kaplan, *Curr. Opin. Solid State Mater. Sci.* **2003**, *7*, 265.
[4] F. G. Omenetto, D. L. Kaplan, *Nat. Photonics* **2008**, *2*, 641.
[5] R. Lewis, *Chem. Rev.* **2006**, *106*, 3762.
[6] M. Heim, D. Keerl, T. Scheibel, *Angew. Chem. Int. Ed.* **2009**, *48*, 2.
[7] Y. Mang, H.-J. Kim, G. Vunjak-Novakovic, D. L. Kaplan, *Biomaterials* **2006**, *27*, 6064.
[8] Z. Guan, *Polym. Int.* **2007**, *56*, 467.
[9] O. Hakimi, D. P. Knight, F. Vollrath, P. Vadgama, *Composites: Part B* **2007**, *38*, 324.
[10] H. Shulha, C. W. P. Foo, D. L. Kaplan, V. V. Tsukruk, *Polymer* **2006**, *47*, 5821.
[11] E. L. Mayes, F. Vollrath, S. Mann, *Adv. Mater.* **1998**, *10*, 801.
[12] C. Li, H.-J. Jin, G. D. Botsaris, D. L. Kaplan, *J. Mater. Res.* **2005**, *20*, 3374.
[13] Q. Dong, H. Su, D. Zhang, *J. Phys. Chem. B* **2005**, *109*, 17 429.
[14] M. Chu, Y. Sun, *Smart Mater. Struct.* **2007**, *16*, 2453.
[15] A. Singh, S. Hede, M. Sastry, *Small* **2007**, *3*, 466.
[16] P. Potiyaraj, P. Kumlangdudsana, S. T. Dubas, *Mater. Lett.* **2007**, *61*, 2464.
[17] P. Wong, S. V. Patwardhan, D. J. Belton, B. Kitchel, D. Anastasiades, J. Huang, R. R. Naik, C. C. Perry, D. L. Kaplan, *Proc. Natl. Acad. Sci.* **2006**, *103*, 9428.
[18] C. Di, J. Jin, Y. Li, X. Kong, K. Wei, J. Yao, *Mater. Sci. Eng. C* **2009**, *29*, 62.
[19] M. L. Gulrajani, D. Gupta, S. Periyasamy, S. G. Muthu, *J. Appl. Polym. Sci.* **2008**, *108*, 614.
[20] S. Dubas, P. Kumlangdudsana, P. Potiyaraj, *Colloids Surf. A* **2006**, *289*, 105.
[21] S. Gupta, M. Hunter, P. Cebe, J. M. Levitt, D. L. Kaplan, I. Georgakoudi, *Biomaterials* **2008**, *29*, 2359.
[22] D. M. Fox, P. Fylstra, M. Hanley, P. C. Trylove, S. Bellayer, J. W. Gilman, H. C. De Long, *ECS Trans.* **2007**, *3*, 11.
[23] S. Zhou, H. Peng, X. Yu, X. Zheng, W. Cui, Z. Zhang, X. Li, J. Wang, J. Weng, W. Jia, F. Li, *J. Phys. Chem. B* **2008**, *112*, 11 209.
[24] X.-X. Feng, L.-L. Zhang, J.-Y. Chen, Y.-H. Guo, H.-P. Zhang, C.-I. Jia, *Int. J. Biol. Macromol.* **2007**, *40*, 105.
[25] D. Blond, D. N. McCarthy, W. J. Blau, J. N. Coleman, *Biomacromolecules* **2007**, *8*, 3973.
[26] S.-M. Lee, E. Pippel, U. Gösele, C. Dresbach, Y. Qin, C. V. Chandran, T. Bräuniger, G. Hause, M. Knez, *Science* **2009**, *324*, 488.
[27] T. Furuzono, A. Kishida, J. Tanaka, *J. Mater. Sci: Mater. Med.* **2004**, *15*, 19.
[28] C. Jiang, V. V. Tsukruk, *Adv. Mater.* **2006**, *18*, 829.
[29] C. Jiang, V. V. Tsukruk, *Soft Matter* **2005**, *1*, 334.
[30] C. Jiang, M. E. McConney, S. Singamaneni, E. Merrick, Y. Chen, J. Zhao, L. Zhang, V. V. Tsukruk, *Chem. Mater.* **2006**, *18*, 2632.
[31] C. Jiang, S. Markutsya, Y. Pikus, V. V. Tsukruk, *Nat. Mater.* **2004**, *3*, 721.
[32] E. Kharlampieva, J. M. Slocik, T. Tsukruk, R. R. Naik, V. V. Tsukruk, *Chem. Mater.* **2008**, *20*, 5822.
[33] Z. Tang, Y. Wang, P. Podsiadlo, N. A. Kotov, *Adv. Mater.* **2006**, *18*, 3203.
[34] P. Hammond, *Adv. Mater.* **2004**, *16*, 1271.
[35] X. Wang, H. J. Kim, P. X. Hu, P. Matsumoto, D. L. Kaplan, *Langmuir* **2005**, *21*, 11 335.
[36] C. Jiang, X. Wang, R. Gunawidjaja, Y.-H. Lin, M. Gupta, D. L. Kaplan, R. R. Naik, V. V. Tsukruk, *Adv. Funct. Mater.* **2007**, *17*, 2229.
[37] S. Srivastava, N. Kotov, *Acc. Chem. Res.* **2008**, *41*, 1831.
[38] C. Jiang, S. Markutsya, H. Shulha, V. V. Tsukruk, *Adv. Mater.* **2005**, *17*, 1669.
[39] R. Gunawidjaja, H. Ko, C. Jiang, V. V. Tsukruk, *Chem. Mater.* **2007**, *19*, 2007.
[40] R. Gunawidjaja, C. Jiang, S. Peleshanko, M. Ornatska, S. Singamaneni, V. V. Tsukruk, *Adv. Funct. Mater.* **2006**, *16*, 2024.
[41] R. Gunawidjaja, C. Jiang, H. Ko, V. V. Tsukruk, *Adv. Mater.* **2006**, *18*, 2895.
[42] Y. Wang, Z. Tang, P. Podsiadlo, Y. Elkasabi, J. Lahann, N. A. Kotov, *Adv. Mater.* **2006**, *18*, 518.
[43] L. F. Drummy, H. Koerner, K. Farmer, A. Tan, B. L. Farmer, R. A. Vaia, *J. Phys. Chem. B* **2005**, *109*, 17 868.
[44] Z. Tang, N. A. Kotov, S. Magonov, B. Ozturk, *Nat. Mater.* **2003**, *2*, 413.
[45] P. Podsiadlo, Z. Liu, D. Paterson, P. P. Messersmith, N. Kotov, *Adv. Mater.* **2007**, *19*, 949.
[46] P. Podsiadlo, A. K. Kaushik, B. S. Shim, A. Agarwal, Z. Tang, A. Waas, E. M. Arruda, N. A. Kotov, *J. Phys. Chem. B* **2008**, *112*, 14 359.
[47] P. Podsiadlo, A. K. Kaushik, E. M. Arruda, A. M. Waas, B. S. Shim, J. Xu, H. Nandivada, B. G. Pumplin, J. Lahann, A. Ramamoorthy, N. A. Kotov, *Science* **2007**, *318*, 80.
[48] P. Podsiadlo, S. Paternel, J.-M. Rouillard, Z. Zhang, J. Lee, J.-W. Lee, E. Gulari, N. A. Kotov, *Langmuir* **2005**, *21*, 11 915.
[49] G. Mehla, M. Kiel, J. W. Lee, N. A. Kotov, J. Lindermann, S. Takayama, *Adv. Funct. Mater.* **2007**, *17*, 2701.
[50] J. L. Lutkenhaus, E. A. Olivetti, E. A. Verploegen, B. M. Cord, D. R. Sadoway, P. T. Hammond, *Langmuir* **2007**, *23*, 8515.
[51] J. Cho, K. Char, J.-D. Hong, K.-B. Lee, *Adv. Mater.* **2001**, *13*, 1076.
[52] P. A. Chiarelli, M. S. Johal, J. L. Casson, J. B. Roberts, J. M. Robinson, H.-L. Wang, *Adv. Mater.* **2001**, *13*, 1167.
[53] C. Jiang, S. Markutsya, V. V. Tsukruk, *Adv. Mater.* **2004**, *16*, 157.
[54] D. Zimnitsky, V. V. Shevchenko, V. V. Tsukruk, *Langmuir* **2008**, *24*, 5996.
[55] V. V. Tsukruk, *Prog. Polym. Sci.* **1997**, *22*, 247.
[56] U.-J. Kim, J. Park, C. Li, H.-J. Jin, R. Valluzzi, D. L. Kaplan, *Biomacromolecules* **2004**, *5*, 786.
[57] S. Markutsya, C. Jiang, Y. Pikus, V. V. Tsukruk, *Adv. Funct. Mater.* **2005**, *15*, 771.
[58] C. Jiang, S. Singamaneni, E. Merrick, V. V. Tsukruk, *Nano Lett.* **2006**, *6*, 2254.
[59] P. Podsiadlo, M. Michel, J. Lee, E. Verpoegen, N. Wong Shri Kam, V. Ball, J. Lee, Y. Qi, J. Hart, P. T. Hammond, N. A. Kotov, *Nano Lett.* **2008**, *8*, 1762.
[60] P. Podsiadlo, Z. Tang, B. S. Shim, N. A. Kotov, *Nano Lett.* **2007**, *7*, 1224.
[61] E. Kharlampieva, D. Zimnitsky, M. Gupta, K. N. Bergman, D. L. Kaplan, R. R. Naik, V. V. Tsukruk, *Chem. Mater.* **2009**, *21*, 2696.
[62] G. W. Beall, D. S. Sowersby, R. D. Roberts, M. H. Robson, L. K. Lewis, *Biomacromolecules* **2009**, *10*, 105.
[63] J. Zhang, X. Li, X. Sun, Y. Li, *J. Phys. Chem. B* **2005**, *109*, 12 544.
[64] V. V. Tsukruk, *Rubber Chem. Technol.* **1997**, *70*, 430.
[65] V. V. Tsukruk, D. H. Reneker, *Polymer* **1995**, *36*, 1791.
[66] C. M. Stafford, C. Harrison, K. L. Beers, A. Karim, E. J. Amis, M. R. Vanlandingham, H. C. Kim, W. Volksen, R. D. Miller, E. E. Simonyi, *Nat. Mater.* **2004**, *3*, 545.
[67] A. J. Nolte, M. F. Rubner, R. E. Cohen, *Macromolecules* **2005**, *38*, 5367.

WILEY InterScience® DISCOVER SOMETHING GREAT
© 2010 WILEY-VCH Verlag GmbH & Co. KGaA, Weinheim